J Mater Sci (2007) 42:1529–1541
DOI 10.1007/s10853-006-0745-9

Severe plastic deformation (SPD) and nanostructured materials by machining

Srinivasan Swaminathan · M. Ravi Shankar · Balkrishna C. Rao · W. Dale Compton · Srinivasan Chandrasekar · Alexander H. King · Kevin P. Trumble

Received: 30 May 2006 / Accepted: 31 July 2006 / Published online: 4 January 2007

Abstract Large plastic strains between 1 and 15 can be imposed in chips formed by plane-strain (2-D) machining of metals and alloys. This approach has been used to examine microstructure changes induced by large strain deformation in model systems—copper and its alloys, precipitation-hardenable aluminum alloys, high-strength materials such as titanium, Inconel 718 and 52100 steel, and an amorphous alloy. It is shown that materials with average grain sizes in the range of 60 nm–1 μm can be created by varying the parameters of machining, which in turn affects the deformation processes. Furthermore, a switch-over from an elongated subgrain microstructure to an equi-axed nanocrystalline microstructure, with a preponderance of large-angle grain boundaries, has been demonstrated at the higher levels of strain in several of these materials. This switch-over can be readily controlled by varying the deformation conditions. Dynamic recrystallization has been demonstrated in select material systems under particular conditions of strain and temperature. This study may be seen as providing an important bridge between furthering the understanding of microstructural refinement by large strain deformation and the practical utilization of nanostructured materials in structural and mechanical applications. Conventional plane-strain machining has been shown to be a viable SPD method for examining the underlying processes of very large strain deformation.

S. Swaminathan · B. C. Rao · W. D. Compton · S. Chandrasekar (✉)
Center for Materials Processing and Tribology, School of Industrial Engineering, Purdue University, West Lafayette, IN 47907, USA
e-mail: chandy@ecn.purdue.edu

M. Ravi Shankar
Department of Industrial Engineering, University of Pittsburgh, Pittsburgh, PA 15261, USA

A. H. King · K. P. Trumble
School of Materials Engineering, Purdue University, West Lafayette, IN 47907, USA

Introduction

Interest in ultra-fine grained (UFG) materials, which exhibit significantly enhanced mechanical properties, has focused renewed attention on the use of severe plastic deformation (SPD) as a means for achieving microstructure refinement in metals and alloys. The role of deformation in microstructure refinement is best highlighted in the pioneering studies of Embury and Fisher [1] on deformation of pearlite, and Langford and Cohen [2] on iron. Langford and Cohen [2], for example, imposed large plastic strains in iron by repeated passes of wire drawing and found the microstructure of the deformed iron wire to be composed of grains and dislocation substructures with sizes in the sub-micrometer range. Furthermore, there was a significant increase in the flow stress of the wire. The use of similar SPD approaches to realize and study microstructure refinement has received an impetus in recent years from the work of Segal et al. [3] and others [4–7]. In these SPD approaches, large shear strains ($\gamma \geq 4$) were imposed, by the cumulative application of plastic deformation, using multiple passes of deformation processing such as equal channel angular extrusion (ECAE), drawing, rolling, or high-pressure torsional straining (HPT). While these SPD methods

are capable of producing bulk nanostructured materials and have provided insights into mechanisms of microstructure refinement, they possess some limitations. First, multiple passes of deformation are needed to create the large plastic strains. Second, moderate and high-strength alloys are difficult to deform in this manner at ambient temperature due to constraints imposed by the forming equipment, including durability of the tools and dies. Lastly, there are uncertainties pertaining to knowledge and control of deformation parameters.

An attractive route for imposing very large plastic strains in a single pass of deformation, while overcoming the aforementioned limitations, is the process of chip formation by machining. Large plastic strains experienced by a chip during its creation by machining result in significant microstructure refinement, including the creation of nanostructured materials [8–10]. This suggests an alternative SPD approach for studying microstructure changes at the micro- and nano-scales. We describe below important aspects of the large strain deformation field in machining. The features of this SPD approach are then illustrated by its application to the study of formation of UFG and nanocrystalline microstructures in various alloys.

Deformation field in machining

SPD results from chip formation even in its simplest manifestation, i.e., plane-strain (2-D) machining (Fig. 1). Plane-strain machining is characterized by a sharp, wedge-shaped tool that removes a preset depth of material (a_o) by moving in a direction perpendicular to its cutting edge. Chip formation occurs by concentrated shear in a narrow deformation zone, often idealized by a plane called the shear plane (Fig. 1). The geometry of the deformation zone and shear strain are determined by the shear angle (φ) and the rake angle (α). The shear strain (γ) imposed in the chip is given by [11, 12]

$$\gamma = \frac{\cos\alpha}{\sin\phi\cos(\phi-\alpha)} \tag{1}$$

where φ is calculated from a measurement of a_o and a_c as

$$\tan(\phi) = \frac{\frac{a_o}{a_c}\cos(\alpha)}{1-\frac{a_o}{a_c}\sin(\alpha)} \tag{2}$$

The principal machining variables controlling the deformation are a_o, V_o, and α. These variables affect the shear deformation in a manner analogous to the action of dies in forging or extrusion. As suggested by Eq. (1), the shear strain (γ) can be varied by varying the rake angle. Additionally, the coefficient of friction between the tool and chip influences the shear angle, and hence, the strain [12, 13]. This coefficient can be varied by a factor of up to four using a novel modulation-assisted machining technique that facilitates lubrication of the tool-chip interface [14]. Since the speed of machining (V_o) influences the deformation zone temperature and strain rate, by cutting at very low speeds (~100 mm/s) this temperature can be kept only marginally above the ambient temperature while imposing large plastic strains. Plastic shear strains in the range of 1–15 and strain rates of up to 1×10^5 s^{-1} can be generated with appropriate machining conditions [12].

In passing, it is interesting to note that the deformation field in plane-strain ECAE is a special case of the deformation field prevailing in machining, namely

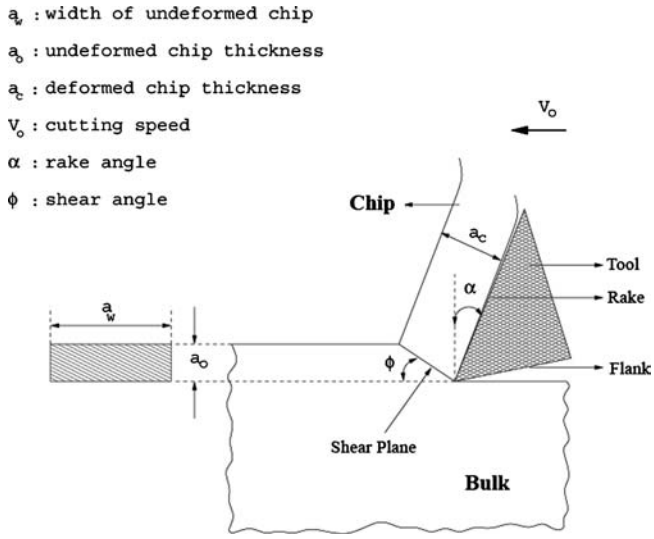

Fig. 1 Schematic of plane strain (2D) machining and associated geometric parameters. The shear plane angle (φ) together with the rake angle (α) determine the average shear strain and the deformation field

it corresponds to $a_o = a_c$ in Fig. 1. Thus, the strain imposed in each deformation pass in plane-strain ECAE may be obtained by setting $a_o = a_c$ and α to the appropriate value dictated by the die angle, in Eqs. (1) and (2). This makes it possible to compare and correlate results from the two techniques in a meaningful manner.

Experimental procedures

Chips of a variety of commercially pure metals and alloys were produced by plane-strain machining for the purpose of examining the effects of large strain deformation. Typical chip samples were 100–3000 μm in width, 100–1000 μm in thickness and at least 5 mm in length. High speed steel (HSS) tools of different rake angles were used to impose varying levels of strain in the chip in materials of low to moderate initial strength. The harder metals and alloys, viz., titanium, Inconel 718 and 52100 steel, were machined with ceramic or cubic boron nitride tools. Table 1 gives the experimental details such as machining parameters and relevant properties of the initial bulk material. Except in those instances where temperature was an experimental variable, the speed of machining was kept sufficiently low to minimize strain rate effects and any temperature rise during chip formation. In situ measurement of the deformation zone temperature made using IR thermography confirmed that the temperature rise in low-speed machining was less than 50 °C.

The shear strain (γ) in the chip was calculated using Eqs. (1) and (2). Inherent in this calculation is the assumption that the deformation zone can be approximated as a shear plane. The shear angle (φ) was obtained from Eq. (2) using a_o, and an average value for a_c, the average value of a_c being obtained from ten thickness measurements made on the chips.

The microstructure of the chips and some of the bulk specimens was characterized using a JEOL 2000FX Transmission Electron Microscope (TEM) operating at 200 kV. For this purpose, chip samples and control samples from the bulk material were prepared either by an electrolytic jet thinning technique or by a wedge-polishing technique. In the electrolytic jet thinning technique, the samples were first ground to a thickness of ~100 μm using an abrasive polishing wheel. Three-millimeter diameter disks were then punched out of the

Table 1 Experimental parameters

Material and composition (by weight)	Bulk initial state	Vickers hardness (kg/mm^2)	Machining parameters	Electro-polishing parameters for TEM samples
OFHC copper (99.98%)	Annealed at 400 °C (4 h), Grain size: 96 μm	57	Tool: HSS, α: +50° to –40°, a_o: 0.1 mm, a_w: 3.8 mm, V_o: 18.3 mm/s–1313.3 mm/s, **γ: 2.9 to 19.9**	46%H_3PO_4 + 56%H_2O (by volume), 20 °C, 5.5 V, 130 mA
Cu–6.7 at% Al	Cast, cold forged and annealed at 750 °C (2 h), Grain size: 417 μm	97	Tool: HSS, α: +40° to –40°, a_o: 0.1 mm, a_w: 3.8 mm, V_o: 11.7 mm/s–831.7 mm/s, **γ: 3.4–10.9**	46% H_3PO_4 + 56%H_2O (by volume), 20 °C, 6.1 V, 140 mA
Al 6061–T6	As-received, Grain size: 75 μm	110	Tool: HSS, α: +20° to –20°, a_o: 0.2 mm, V_o: 10 mm/s, **γ: 1.7–5.2**	25% HNO_3 + 75% CH_3OH (by volume), –10 °C, 9.5 V, 150 Ma
Al 6061-T6 (solution-treated)	Annealed at 550 °C (10 h), Grain size: 30 μm	72	Tool: HSS, α: +20° a_o: 0.2 mm, V_o: 10 mm/s, **γ: 2.7**	25% HNO_3 + 75% CH_3OH (by volume), –10 °C, 9.5 V, 150 mA
Vitreloy ($Zr_{41.25}$–$Ti_{13.75}$–$Cu_{12.5}$–Ni_{10}–$Be_{22.5}$)	Amorphous		Tool: HSS, α: +10°, a_o: 0.05 mm, V_o: 8.3 mm/s, **γ: 2**	25% HNO_3 + 75% CH_3OH (by volume), –10°C, 9.5 V, 150 mA
AISI 52100 steel	Tempered martensite	9.1 Gpa (Based on nano-indenation)	Tool: Cubic boron nitride, a_o: 0.1 mm, a_w: 3.2 mm, V_o: 2500 mm/s	20% $HClO_4$ + 80% CH_3OH (by volume), 25°C, 40 V, 130 mA
Inconel 718	Solution treated Grain size: 18 μm	280	Tool: Ceramic (Sialon), α: +5(° to –20°, a_o: 0.064 mm, V_o: 450 mm/s, **γ: 2.4–7.8**	25% HNO_3 + 75% CH_3OH (by volume), –10 °C, 9.5 V, 150 mA
Titanium	As-received Grain size: 41 μm	143	Tool: HSS, α: +20° to –20°, a_o: 0.1 mm, V_o: 8.3 mm/s, **γ: 2.0–6.0**	60% CH_3OH + 35% C_4H_9OH + 5% $HClO_4$ (by volume), –30 °C, 40 V

ground samples and were made electron transparent by electrolytic twin-jet thinning on a Struers Tenupol-5 polishing system. The electrolytes and conditions used for preparing TEM specimens, from different materials, by twin-jet thinning are given in Table 1. For the wedge-polishing technique, the specimens were mechanically thinned by abrasive polishing to form shallow wedges. Each wedge was then mounted on a copper slot grid and milled using Argon ions, at low incident angles (<5°), for 5–10 min in a Gatan Model 600 dual ion mill to create an electron transparent specimen. Care was taken to avoid any prolonged heating of the specimens during the mechanical thinning and ion milling in order to ensure the integrity of the microstructure of the chip.

Bright- and dark-field images, along with selected area diffraction patterns (SAD), were taken to analyze grain size, defect structure and subgrain misorientation. The average grain size was determined by sampling 50–100 grains using Heyn's line intercept method. If the aspect ratio, defined as the ratio of the length to width of a grain, of the grains was greater than 2, then the grain was considered as elongated; otherwise the grain was taken to be equi-axed. For those chips with elongated grain microstructures, the mean width of a grain is reported as the grain size.

Some of the chip and bulk samples were polished for microstructure analysis and hardness testing. Hardness measurements were made using Vickers indentation taking care to ensure that the size of an indentation, as measured by its diagonal length, was kept about the same in the bulk and chip samples so as to minimize any uncertainties arising from an indentation 'size effect'. Furthermore, the size of a hardness indentation was kept appropriately smaller than the specimen size to eliminate edge effects. An average value for the hardness was obtained by performing at least 15 indents in each sample.

Results

The utility of machining for introducing a range of strains in a single deformation pass is evident from Fig. 2, which shows the variation of chip shear strain with tool rake angle for oxygen free high conductivity (OFHC) Cu and Al 6061-T6. The shear strain in the 6061-T6 chip is seen to vary between 1.7 with a +20° rake tool and 5.2 for a –20° rake tool and in the copper chip from 2 with a +50° rake tool to 14 with a –20° rake tool.

While the strain values given in Fig. 2 are estimated based on the shear plane model (Eqs. (1) and (2)), the strain field associated with the deformation has only recently been measured directly. This has been done by applying an image correlation method to sequences of high-speed photographic images of material flow through the deformation zone [15]. Figure 3a and b show typical results from these measurements, in the form of velocity and strain rate distributions, respectively, for plane-strain machining of OFHC copper. The change in velocity from that of the bulk to that of the chip occurs over a relatively narrow area in the copper, as shown in Fig. 3a. This region of velocity change may be broadly identified with the deformation zone. The shear strain rate distribution in Fig. 3b, a measure of the strain increment imposed during an incremental advance of the tool, is the true deformation zone and is seen to be very narrow. This suggests that for OFHC copper, the shear plane model of deformation is reasonable. The average shear strain rate in the deformation zone is about 200/s. Additional measurements showed this strain rate to increase linearly with machining speed, indicating that strain rates of ~10^5/s can be realized in chip formation at high speeds (~10 m/s).

The total shear strain imposed in the chip material over its entire history of deformation can be obtained by carrying out a discrete summation of the incremental shear strains along a particle trajectory. Figure 4 shows the cumulative shear strain calculated in this manner at different points along a trajectory ABCD. The magnitude of the shear strain increases monotonically in the narrow region BC before reaching a constant value of ~ 4 in region CD, which corresponds

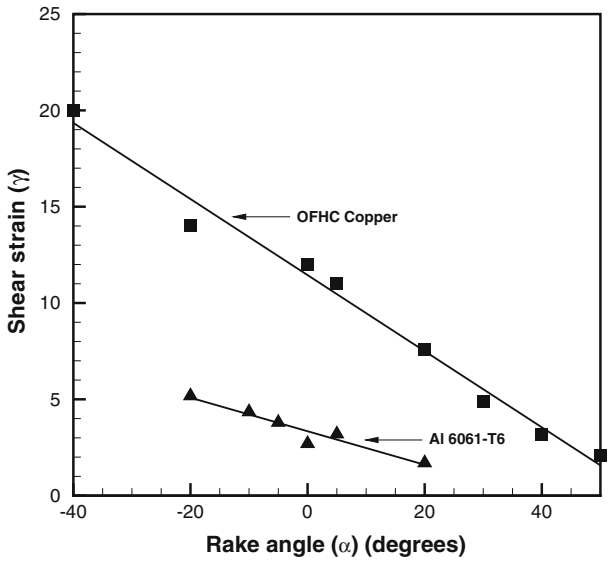

Fig. 2 Variation of shear strain (γ) with tool rake angle (α) for Al 6061-T6 and OFHC copper. The shear strain plotted here is calculated using Eqs. (1) and (2)

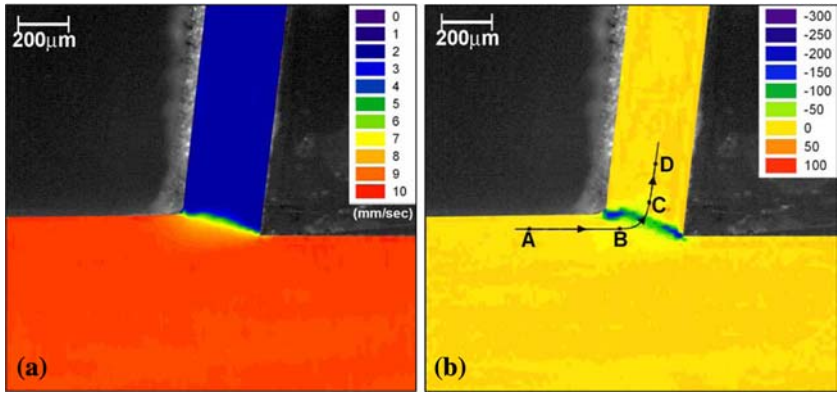

Fig. 3 Deformation field in OFHC copper derived from high-speed image analysis (V_o= 10 mm/s, α = + 10° and a_o = 0.10 mm) (**a**) velocity distribution and (**b**) shear strain rate (strain/s) distribution. The region of maximum shear strain rate may be identified with the deformation zone. ABCD shows a particle trajectory

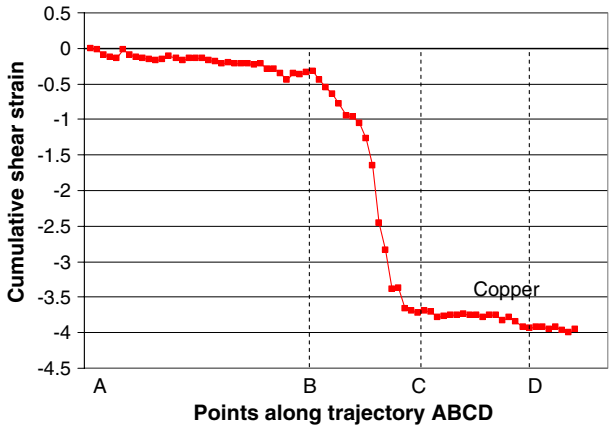

Fig. 4 Cumulative shear strain in copper along trajectory ABCD of Fig. 3(**b**)

to the fully developed chip. This value of 4 for the chip strain is within 15% of the value of 4.7 estimated for using Eq. (1). Similar measurements in other alloys have confirmed the validity of this observation. In this study, the reported strains are all based on the shear plane model and Eqs. (1) and (2).

Microstructure evolution with strain: Cu and Cu–6.7 at% Al

The microstructure of a plastically deformed material is strongly influenced by deformation parameters such as strain, temperature and strain rate. The effect of strain on microstructure, even in low-strength metals and alloys, has been studied only by using a combination of deformation tests or multi-pass deformation processes. Microstructure changes occurring in the earlier stages of plastic deformation ($\gamma < 1$) in copper, for example, have been explored using tension tests [16]. The later stages of plastic deformation ($\gamma \sim 1$–15) have been studied using SPD processes, involving multiple passes of rolling [17], wire drawing [1, 2] and ECAE [18]. In this section, we show, using deformation of OFHC copper and Cu–6.7 at% Al by plane-strain machining as examples, the microstructure and strength (hardness) changes that occur over the shear strain range of 1–15 in single-pass SPD.

Figure 5a–d shows a series of TEM micrographs of OFHC copper chips created with different levels of strain. A range of UFG microstructures and nano-scale dislocation substructures can be seen in these images. The microstructure of the chip created with the lowest strain ($\gamma \sim 3$), shown in Fig. 5a, is seen to be composed almost entirely of dislocation substructures (subgrains) having diffuse boundaries. The subgrains are elongated with a mean width of ~350 nm. At a shear strain of ~5, some of the grain boundaries of the prior bulk material have become corrugated (see at arrows in Fig. 5b). Similar corrugated grain boundaries have been observed at true strain values as low as 0.8 in copper deformed by compression [19]. The microstructure in Fig. 5b is composed of elongated subgrains with a mean width of 150–175 nm; the elongated subgrains show sharper boundaries (compared to Fig. 5a) with little dislocation activity in their interior, thus suggesting the occurrence of dynamic recovery. The microstructure of the $\gamma \sim 11$ chip in Fig. 5c consists of a mixture of elongated and equi-axed nano-scale grains with dislocation-free interiors, suggesting the onset of dynamic recrystallization. The original grain boundaries of the bulk material can no longer be resolved. A further increase in the strain to ~14 results in a purely equi-axed microstructure with a mean grain size of 200 nm (Fig. 5d). The SAD patterns, insets in Fig. 5b and d, indicate that the proportion of large-angle boundaries increases with increasing strain. The switch-over from an elongated subgrain type microstructure, at the lower levels of strain, to the equi-axed UFG microstructures at the higher levels of strain (Fig. 5) has not previously been realized in any single-pass deformation process. Figure 6 summarizes the variation of mean subgrain

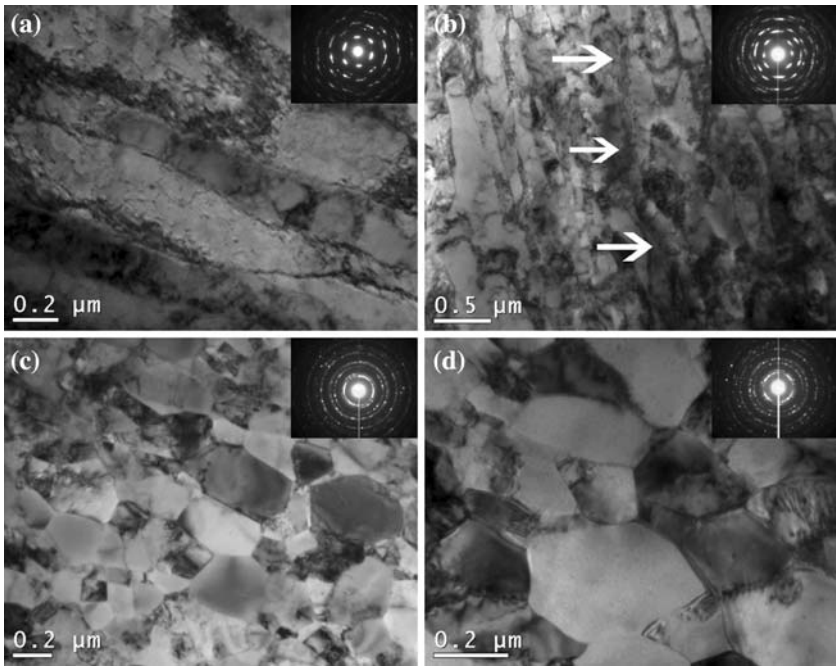

Fig. 5 Bright-field TEM micrographs of OFHC copper chips showing microstructures at different levels of shear strain (**a**) $\gamma \sim 3$ chip showing elongated dislocation structures [length: 1225 nm, width: 335 nm], (**b**) $\gamma \sim 5$ chip showing corrugated original grain boundaries (marked by arrows) and elongated subgrains [length: 725 nm, width: 155 nm], (**c**) $\gamma \sim 11$ chip showing a mixture of elongated subgrains [length: 530 nm, width: 170 nm] and equi-axed grains [250 nm] and (**d**) $\gamma \sim 14$ showing equi-axed nano-scale grains [215 nm] with few dislocations visible in their interior. The inset SAD patterns in figures (**b**) and (**d**) indicate the fraction of large-angle boundaries increases with increasing strain. Low speed cutting, V_o = 18.3 mm/s

size with shear strain for OFHC copper. The width of the elongated subgrains is seen to have a minimum value of ~150 nm at a shear strain of ~8. These microstructural observations are consistent with results from multi-pass SPD of copper [18].

The Vickers hardness (strength) of copper chips as a function of shear strain is also shown in Fig. 6. The hardness of the UFG chips (150 kg/mm^2) is nearly three times that of the bulk copper (57 kg/mm^2). Furthermore, no hardness anisotropy was seen in the chips. The significant increase in hardness of chips at the lower shear strains ($\gamma < 5$), where original grain boundaries are still visible in the TEM micrograph (Fig. 5b), suggests that the initial strengthening is largely due to creation, multiplication and interaction of dislocations. With further increase in the strains, dynamic recovery occurs resulting in annihilation and rearrangement of dislocations; but the creation of nano-scale grains helps maintain the hardness of the copper chips at 150 kg/mm^2. Thus, the hardening observed at the lower strains is likely a consequence of the fine dislocation substructures or subgrains, while grain size strengthening is likely the principal contributor to the enhanced hardness at the higher strains.

Chips were also created with different levels of strain from copper-based solid solutions in order to study the interactive effects of strain, stacking fault energy (SFE) and solutes on microstructure evolution and hardening. Figure 7a–c shows TEM micrographs of chips cut with the different strains from low SFE

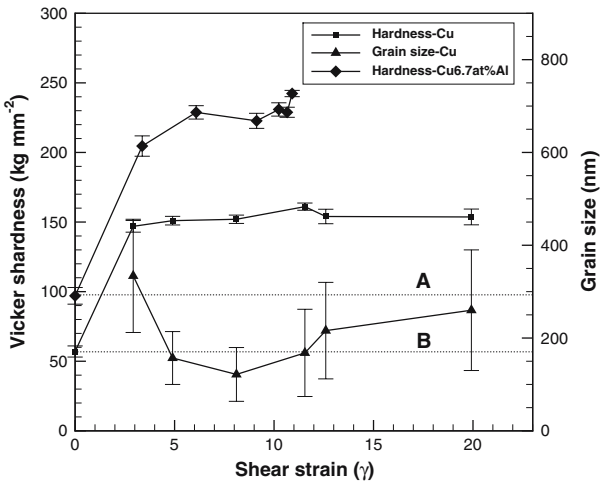

Fig. 6 Vickers hardness of Cu and Cu–6.7 at% Al chips and grain size of Cu chips as a function of imposed shear strain. The dotted lines marked A and B correspond to the initial bulk hardness values of Cu–6.7 at% Al and Cu, respectively. The average width is used to describe the subgrain size of the elongated structures

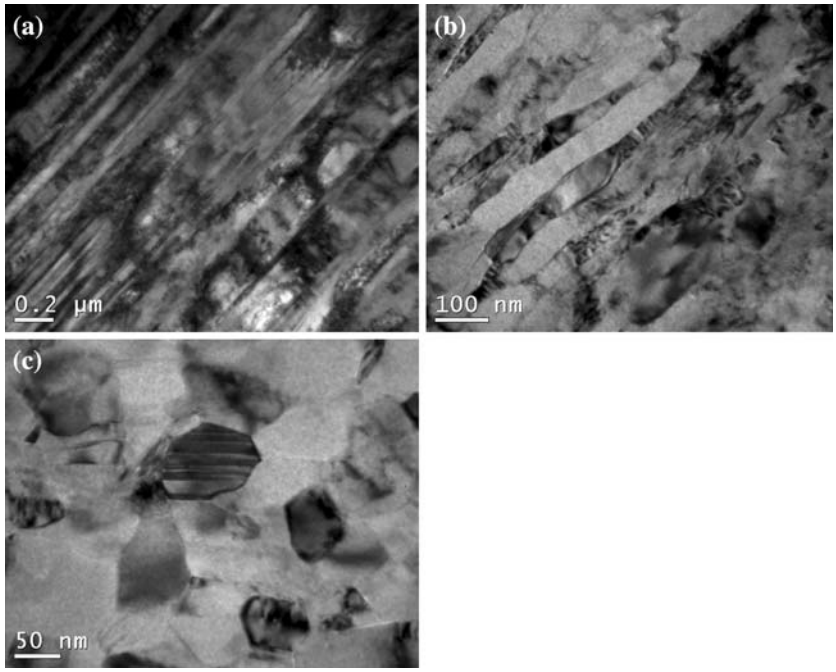

Fig. 7 Bright field TEM micrographs of Cu–6.7 at% Al chips created at different levels of shear strain (**a**) γ ~3 chip showing long twins [width: 75 nm], (**b**) γ ~ 9 chip showing elongated subgrains [length: 215 nm, width: 65 nm] and (**c**) γ ~ 10 chip showing equi-axed nano-scale grains [110 nm] with deformation twins seen in some of the grains' interior. V_o = 11.7 mm/s

Cu–6.7 at% Al, a single-phase solid solution. At the lower shear strains ($\gamma \sim 3$), the microstructure is composed primarily of elongated twins with an average width of ~75 nm. Tilting experiments in the TEM confirmed that the elongated twins extended through the entire length of the electron transparent regions. The twin-type microstructure gives way to elongated subgrain structures at a shear strain of ~6. With further straining, there is a switch-over from the elongated subgrain microstructure to a mixture of elongated nano-scale structures and equi-axed nano-scale grains, followed by a microstructure that is composed entirely of equi-axed nano-scale grains of ~100 nm size with high misorientations (Fig. 7c). The equi-axed microstructure is likely a consequence of deformation-induced recrystallization. The microstructure evolution with strain in the Cu–6.7 at% Al is seen to parallel that of the copper, albeit that the equi-axed grains observed at the higher levels of strain in the solid solution have a smaller grain size.

When the deformation zone temperature is increased by increasing the cutting speed, the microstructure is seen to be composed mainly of equi-axed grains at a shear strain of ~10, see Fig. 8. The mean grain size is ~300 nm which is somewhat greater than that (~100 nm) observed at the same level of strain under conditions of minimal temperature rise (Fig. 7c); this effect of temperature is also similar to that observed in copper. However, the presence of solutes in the Cu–6.7 at% Al alloy inhibits the formation of micrometer-sized grains in these chips, unlike in copper.

The Vickers hardness of the Cu–6.7 at% Al chips is much greater than that of the Cu chips, as may be seen from Fig. 6. The hardness value for the Cu–6.7 at% Al chips created at the higher shear strains is ~220 kg/mm^2 as compared to a value of ~150 kg/mm^2 for the UFG copper; this hardness difference reflects the contribution arising from solid-solution strengthening.

The above observations clearly demonstrate the variety of UFG and nano-scale microstructures that can be realized by varying machining and, hence, deformation parameters. Furthermore, the

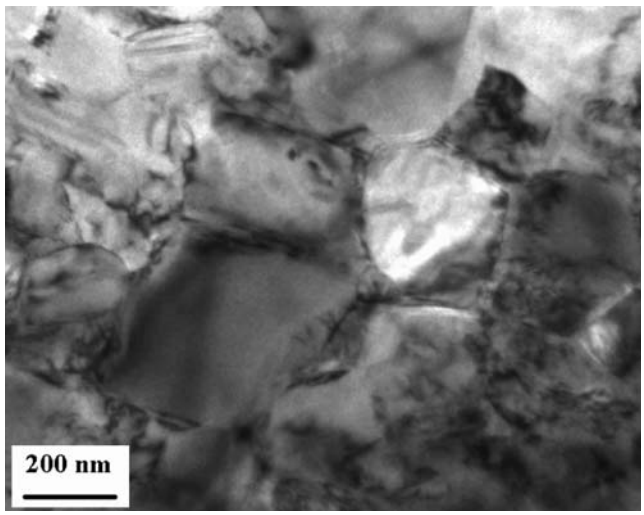

Fig. 8 Bright field TEM micrograph of γ ~ 10 Cu–6.7 at% Al chip cut at higher speed showing equi-axed grains [310 nm]. V_o = 831.7 mm/s

switch-overs in microstructure with strain can be realized in a single pass of deformation and are controllable by adjusting the machining parameters.

Precipitation-hardening aluminum alloys

Precipitation-hardening aluminum alloys (e.g., Al 6061, Al 7075, Al 2024) with nanocrystalline microstructure are of special interest due to their potential for being thermally stable at higher temperatures [7, 20–22]. The precipitate phases in these alloys are expected to not only modify the micromechanics of large strain deformation, but also stabilize the microstructure by pinning the grain boundaries, thus inhibiting coarsening of the microstructure. Consolidation of UFG chips by conventional powder metallurgy techniques to fabricate bulk forms is likely to involve some heating. Thus, thermal stability of the nanocrystalline microstructure is a necessary characteristic for retention of the superior mechanical properties in the consolidated bulk. Here, the creation of thermally stable UFG microstructures in Al 6061 by machining is pursued through two processing routes.

The first route involves deformation of the Al 6061-T6 bulk material by machining to create an UFG microstructure. Aluminum 6061-T6 is characterized by an optimal, fine dispersion of precipitates. It is expected that deformation of such a material by chip formation will lead to a microstructure that is stabilized by the precipitates inherited from the bulk. Figure 9a and b shows the microstructure resulting from large strain deformation of Al 6061-T6. The initial grain size in the bulk material is ~75 μm and the bulk Al 6061-T6 hardness is 110 kg/mm^2. It can be seen in Fig. 9a that relatively coarse (~150 nm wide) and high-aspect ratio grains result from the deformation of the Al 6061-T6 to relatively low values of shear strain (~1.7). However, a very fine microstructure composed of equi-axed grains typically ~80 nm in size is obtained in the chips created by deforming the Al 6061-T6 to larger shear strains of ~3.2 (Fig. 9b).

An annealing study aimed at characterizing the thermal stability of the chips was performed at 175 °C, the common ageing temperature for Al 6061. While the UFG chips are observed to gradually soften during this heat treatment, they are still generally harder than the bulk even after prolonged annealing (Fig. 10). Figure 11a shows the microstructure of the $\gamma \sim 3.2$ chips after 1 h of annealing at 175 °C. It may be noted that the microstructure has coarsened compared to the as-machined chips and this coarsening is associated with a relatively rapid decrease in Vickers hardness from an initial value of ~150 kg/mm^2 for the as-machined chip to ~140 kg/mm^2 after 1 h of annealing. Prolonged annealing beyond 1 h at 175 °C is associated with a much slower decline in the hardness. It can be seen from Fig. 10 that the chips continue to be harder than the bulk even after 10 h at 175 °C.

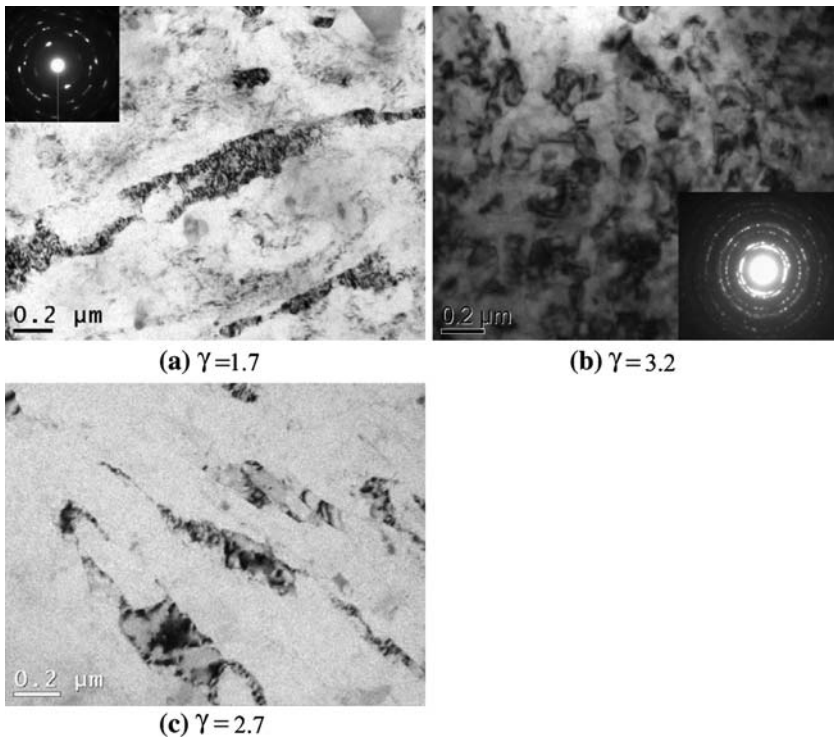

Fig. 9 Bright-field TEM micrographs of Al 6061 chip deformed to different levels of shear strain. (**a**) and (**b**) show microstructure of chips cut from the 6061-T6 bulk material and (**c**) microstructure of chip cut from solution-treated bulk material

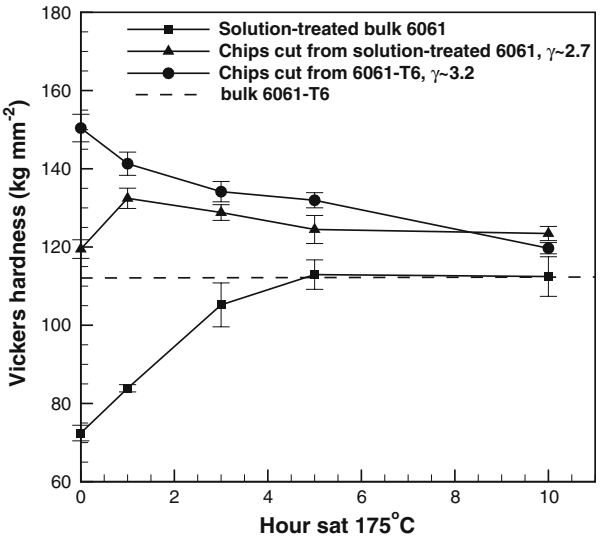

Fig. 10 Vickers hardness versus annealing time at 175 °C. Indentation load is 50 g

The second route for the production of UFG Al 6061 involves deformation of the material in the solution-treated state; this state is characterized by a single-phase microstructure that is devoid of any strengthening precipitates. Deformation of the solution-treated material to a shear strain of ~2.7 yields an UFG microstructure that is typically composed of elongated grains as shown in Fig. 9c. This grain refinement is associated with significant hardening vis-á-vis the undeformed solution-treated bulk (Fig. 10). Upon ageing at 175 °C, it is seen that the chips cut from solution-treated bulk further gain in strength (hardness) reaching a peak-hardness value of ~135 kg/mm^2 after 1 h, before gradually softening. Typically, the undeformed, bulk solution-treated 6061 requires ageing for 8–10 h at 175 °C to achieve a peak-hardness value of ~110 kg/mm^2. The large defect concentration in the severely strained chips accelerates the precipitation process. It can be seen in Fig. 11b that the aged chip material retains a relatively fine microstructure and is strengthened and stabilized by a fine dispersion of precipitates that form rapidly in the strained matrix during the ageing process.

It is interesting to note that for the same heat-treatment time and temperature, the grain size and the hardness value obtained from ageing the chips cut from the solution treated material is similar to that obtained from annealing of the UFG chips cut from the Al 6061-T6 alloy. This is an instance of two distinct processing routes leading to a similar end product—a precipitation-hardened alloy with nanocrystalline microstructure that shows significant resistance to coarsening during thermal treatment.

High-strength metals and alloys

The machining technique is quite applicable for studying the development of UFG microstructures by SPD in technologically important, high-strength materials like titanium, Inconel 718 and 52100 steel. These alloys are difficult to deform to large strains at ambient temperatures by the usual SPD processes. The microstructures resulting from application of shear strains in the range of 2–10 have been analyzed.

In commercially pure Ti, a shear strain of ~3, obtained with +20° rake angle tool, led to significant grain refinement. The microstructure of this chip in Fig. 12a is seen to be comprised of sub-100 nm grains that are considerably misoriented with respect to one another. The grain misorientations were qualitatively judged from the SAD pattern shown as an inset in Fig. 12a. The hardness of this chip is 230 kg/mm^2, nearly 70% greater than that of the bulk (~140 kg/mm^2). With a larger value of strain ($\gamma \sim 6$), the resulting microstructure was found to be negligibly different from that of the $\gamma \sim 3$ chips. Its hardness value was ~247 kg/mm^2, only slightly higher than that of the chip created at the lower strain, indicating the oft-observed phenomenon of diminishing incremental microstructure refinement and flow-stress saturation at large values of strain.

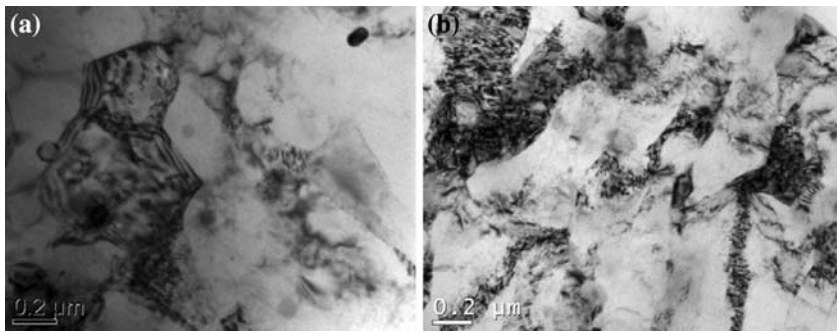

Fig. 11 Bright-field TEM micrographs of (**a**) $\gamma = 3.2$ chip cut from Al 6061-T6 bulk sample and annealed for 1 h and (**b**) $\gamma = 2.7$ chip cut from solution-treated Al 6061 bulk sample and annealed for 1 h

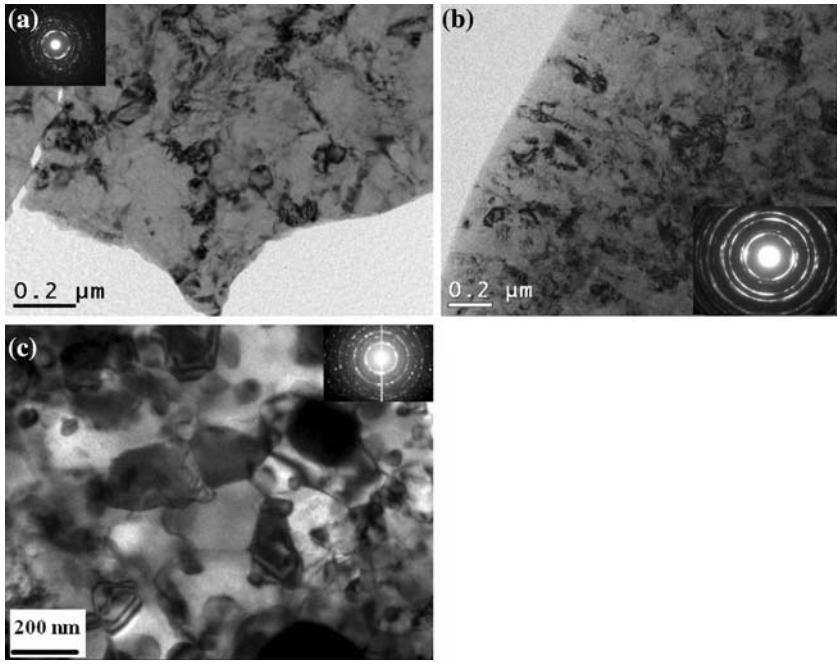

Fig. 12 Bright-field TEM micrographs of chips cut from (**a**) commercially pure Ti, $\gamma \sim 3$, grain size: 80 nm, (**b**) Inconel 718, $\gamma \sim 8$, grain size: 120 nm and (**c**) 52100 steel with equi-axed nano-scale ferrite grains [330 nm] and dispersed carbide particles

Similar SPD studies in Inconel 718 involved imposition of shear strains of 2.4 and 8 with attendant refinement of the microstructure. There was no significant difference between the hardness values for the two cases—550 kg/mm^2 and 569 kg/mm^2, respectively. These values are twice as great as that of the bulk Inconel 718. Figure 12b is a TEM micrograph of the $\gamma \sim 8$ chip. Particularly striking is the SAD pattern (shown as an inset) which is comprised of nearly uniform rings around the central beam, indicating a significantly misoriented microstructure composed of ultra-fine grains with size ~100 nm.

The capability offered by machining for the study of large strain deformation in difficult-to-deform materials is further reinforced by the TEM micrograph in Fig. 12c, which shows a multi-phase UFG microstructure resulting from large strain deformation of 52100 steel with an initial tempered martensite microstructure. Highly misoriented, ~330 nm sized ferrite grains that are reinforced by a dispersion of fine carbide particles can be seen. Nanoindentation of the UFG chip showed its hardness to be ~13 GPa as compared to a value of ~9 GPa for the bulk material. The hardness of 13 GPa is similar to that of patented steel wire, one of the strongest steel structures known [23].

Large strain deformation of an amorphous alloy

Because of its capability to impose controlled large strains over macroscopic regions, the machining approach was used to further examine the possibility of large strain deformation of amorphous alloys at room temperature. For this purpose, a commonly available, Zr-based amorphous alloy (Vitreloy-1: $Zr_{41.25}$–$Ti_{13.75}$–$Cu_{12.5}$–Ni_{10}–$Be_{22.5}$) was deformed to a shear strain of ~2 by plane-strain machining under quasi-static conditions. This amorphous alloy is highly stable in that it has a recrystallization temperature of ~710 K [24] which is substantially higher than that of most other amorphous alloys. The machining parameters used were a cutting velocity of 8.3 mm/s, an undeformed chip thickness (a_o) of 50 μm and a tool rake angle of +10°. Such a low cutting velocity was selected to ensure quasi-static deformation and to minimize heating of the chip sample during the imposition of large strains. A vegetable oil based fluid was used to minimize any frictional heating.

Partially formed Vitreloy chips, still attached to the bulk sample, were created in a specially devised experiment in which the machining was interrupted and studied in a JEOL JSM-5300 Scanning Electron Microscope (SEM) in order to discern the external morphology of the chips vis-à-vis the undeformed, bulk Vitreloy. Figure 13a and b is SEM pictures of the typical morphology of an as-machined chip of Vitreloy-1 produced by the 2-D machining. The micrographs reveal a fine, micrometer-scale, shear band pattern, which is seen to encompass the entire chip. The spacing between the shear bands is ~1 μm as may be seen from Fig. 13b. Such a shear band pattern is a generally

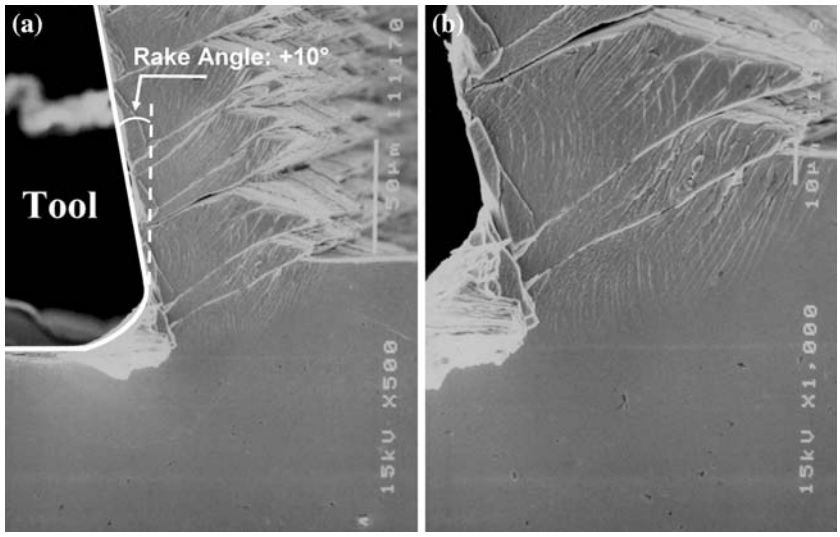

Fig. 13 SEM micrographs of a partially formed chip of Vitreloy-1 showing micro-scale shear bands. (**a**) Low-magnification image showing a partially formed chip with the orientation of the tool indicated, and (**b**) higher-magnification image illustrating dense network of shear bands (band spacing ~1 μm) encompassing the chip

observed characteristic of amorphous alloys deformed at room temperature [25, 26].

In TEM studies of the severely deformed chips, we found no evidence of recrystallization of the amorphous material. We anticipate that the deformation temperature and strain imposed might be insufficient to lead to recrystallization within the shear bands in the amorphous material. However, it is noteworthy that an amorphous alloy, typically characterized by limited ductility can be deformed to large values of shear strain at room temperature. It is presumed that a significant portion of these large strains, imposed during chip formation, are accommodated within the dense network of shear bands that characterizes the severely deformed chip.

Implications

The experimental observations have shown that plane strain machining offers a simple route for studying the effects of SPD on microstructure in a variety of alloys ranging from low to high initial strength. Furthermore, the results show that chip formation by machining is a viable process for making nanostructured materials.

Large strain deformation

A range of shear strains and variety of resulting microstructures have been produced in the chip through appropriate choice of the tool rake angle. However, application of the same rake angle to two different materials can lead to different shear strains in the chip. This difference is shown in Fig. 2, where a zero-degree rake angle tool produced a shear strain of ~11 in copper and ~3 in Al 6061-T6. This is not surprising considering that, in machining, the geometry of the deformation field is not defined a priori. This does not imply that the strains cannot be introduced in a controllable manner. From data such as in Fig. 2, it is possible to determine directly the relation between the tool rake angle and the shear strain in the chip for a specific material; this relation can then be used to impose a controlled level of strain in the chip. The ability to characterize quantitatively the deformation field parameters in machining, such as strain and strain rate (e.g., Figs. 3 and 4) allows for an examination of the interactive effects of these parameters on microstructure refinement and work-hardening in materials.

Figure 3b shows that the maximum shear strain rate in the deformation zone when cutting copper at a speed of 10 mm/s is ~200/s. Based on our recent measurements that show the strain rate to increase linearly with increasing cutting speed, the shear strain rate at a cutting speed of 10,000 mm/s is estimated at $\sim 2 \times 10^5$/s. Since this range of speeds is realizable in practice, a range of strain rates can be imposed in the deformation zone.

While the temperature in the deformation zone is also expected to increase with increasing cutting speed, this temperature can be measured using infra-red radiation methods [27]. The interdependence of microstructure on strain rate and temperature can then be studied using the well-known concept of the Zener–Hollomon parameter [28]. Furthermore, by combining modeling of large strain deformation with measurements of the deformation field parameters, it may be feasible to infer the stress-strain behavior of materials at large strains (1–10), high strain rates (10–10^5/s) and elevated temperatures (>0.5 T_M).

Microstructure development

The ability to control the microstructure by varying the deformation conditions in machining has been demonstrated. The minimum grain sizes that have been realized to date in SPD by machining range from ~60 nm in precipitation hardening alloys such as Al 6061-T6 to ~160 nm in pure metals such as copper (Fig. 5). This scale of the microstructure in Al 6061-T6 is somewhat finer than that observed in the same alloy processed by warm ECAE [20]. The addition of small amounts of solute to pure metals is seen to result in smaller grain sizes; for example, the smallest grain size created by the machining in Cu–6.7 at% Al is ~100 nm. Similar observations have been made in other solid solutions of copper. Additional evidence in support of finer-scale microstructures in alloys can be found in observations of ~100 nm sized grains in Inconel 718 created by machining (Fig. 12). This is likely a consequence of the deformation-induced microstructure being stabilized by the solutes and precipitates.

A switch-over has been observed from an elongated UFG microstructure at lower strains to an equi-axed nanocrystalline microstructure, with relatively low density of dislocations, at the higher strains (Figs. 5 and 7). The equi-axed microstructure is likely a consequence of dynamic recrystallization occurring during machining.

The nanostructured chip materials are up to three times harder than the corresponding bulk material in the micro-crystalline form (e.g., Fig. 6). The hardness values of the Cu and Cu–6.7 at% Al chips increase quite steeply with imposed strain, initially, but change negligibly at the higher strains. This is true also for the Al 6061 alloys [29]. The hardness saturation at the relatively low strains occurs even though the microstructure often evolves from an elongated subgrain type structure at the lower strains to an equi-axed fine grained microstructure, with high degree of misorientations, at the higher strains. This suggests that the microstructure contribution to the strengthening is different at the lower (dislocation substructure strengthening) and higher strains (grain size strengthening). While we have not yet measured the ductility corresponding to these two types of microstructures, it is likely that they are different. The equi-axed microstructures are likely to show a greater ductility than the elongated subgrain type microstructures. Tensile tests on the chip samples should provide the answer to this question of microstructure dependence of ductility.

Chip samples several millimeters wide and up to several hundred micrometers thick are easy to create by machining. Miniature tensile specimens can be fashioned out of these ''bulk'' chip samples and used to directly assess intrinsic mechanical properties such as yield stress, ductility, fatigue strength and fracture toughness. Preliminary measurements of the yield strength of an OFHC copper chip sample made in this manner have shown that the enhancement in the strength of the chip relative to the bulk sample is similar to that of the measured increase in the Vickers hardness. The chip samples can also be used to characterize thermal stability of the nanocrystalline and UFG microstructures, as has been done with Al 6061.

Production of nanostructured materials

The experiments have provided clear evidence that nanocrystalline metals and alloys of high strength are formed through a normal machining process. Perhaps more important, this process provides an avenue for the production of nanocrystalline structures in a far wider range of materials and at far lower costs than has been foreseen using other processes. An UFG structure of virtually any metal or alloy can be produced through the same basic process.

Machining is not normally considered a bulk deformation process but, in principle, the size of chips is limited only by machine power. Indeed, chips several millimeters in thickness can be produced from initially low strength alloys using commonly available machine tools. Hence, machining reasonably can be considered among the other bulk SPD processes. The process can be scaled down, as well, giving it wide flexibility, by simply changing cutting parameters.

The availability of large volumes of metal chips, either as byproducts from existing manufacturing operations or from specific chip making processes, offer opportunities to create structural materials with mechanical properties that are influenced by the UFG microstructure of the chips. Various comminution and consolidation processes for converting chips to bulk monolithic and composite components are the subject of on-going research. An important consideration, as in consolidating any nanostructured material, is to limit heating in order to suppress coarsening phenomena. While none of these processes have been fully developed with these starting materials, preliminary results suggest that the opportunity exists to create advanced materials with new and interesting combinations of properties.

Conclusions

The study has established that controlled shear strains in the range of 1–15 can be imposed in the chip in a

single pass of plane-strain machining and the microstructure of the chip is substantially finer than that of the bulk material. Furthermore, the deformation parameters associated with chip formation including strain and strain rate can be related to the machining parameters such as tool rake angle and undeformed chip thickness by direct measurement. Thus, machining provides an experimental framework for studying microstructure refinement by SPD in metals and alloys.

A microstructure composed of equi-axed sub-100 nm grains, with a high degree of grain misorientation, has been demonstrated in various alloys ranging from low to high strength by appropriate selection of the machining parameters. UFG microstructures, both equi-axed and of the elongated subgrain type, have been shown to occur in pure metals and select alloy systems. The hardness (strength) of the UFG and nanocrystalline materials created by machining is significantly greater than that of the corresponding microcrystalline forms.

Chip formation by machining provides an avenue for the production of UFG microstructures in a far wider group of materials and, potentially, at far lower costs than has been foreseen using other processes.

Acknowledgements We would like to thank the Department of Energy (grant 4000031768 via UT-Batelle), Oak Ridge National Laboratory (ORNL), Ford Motor Company, the State of Indiana's 21st Century Research and Technology Fund, the NSF (Grants DMI 0500216 and CMS 0200509) and the USAF–PEWG program (via Anteon Corporation) for supporting this work. Additional thanks are also due Drs. Andrew Sherman (Ford) and Ray Johnson (ORNL) for their encouragement of the studies. SS would like to acknowledge support of a National Research Council Fellowship.

References

1. Embury JD, Fisher RM (1966) Acta Metall 14:147
2. Langford G, Cohen M (1969) Trans ASM 62:623
3. Segal VM, Reznikov VI, Drobyshevskiy AE, Kopylov V (1981) Russ Metall 1:99
4. Valiev RZ, Islamgaliev RK, Alexandrov IV (2000) Prog Mater Sci 45:103
5. Humphreys FJ, Prangnell PB, Bowen JR, Gholinia A, Harris C (1999) Phil Trans R Soc Lond A357:1663
6. Hughes DA, Hansen N (2000) Acta Mater 48(11):2985
7. Horita Z, Fujinami T, Nemoto M, Langdon TG (2000) Metall Mater Trans A31:691
8. Brown TL, Swaminathan S, Chandrasekar S, Compton WD, King AH, Trumble KP (2002) J Mater Res 17(10):2484
9. Swaminathan S, Ravi Shankar M, Lee S, Hwang J, King AH, Kezar RF, Rao BC, Brown TL, Chandrasekar S, Compton WD, Trumble KP (2005) Mater Sci Eng A 410–411:358
10. Ravi Shankar M, Rao BC, Lee S, Chandrasekar S , King AH, Compton WD (2006) Acta Mater 54:3691
11. Merchant ME (1945) J Appl Phys 16:267
12. Shaw MC (1984) Metal cutting principles. Oxford University Press
13. Madhavan V, Chandrasekar S, Farris TN (2000) J Appl Mech 67(1):128
14. Moscoso W, Olgun E, Compton WD, Chandrasekar S (2005) J Trib 127:238
15. Lee S, Hwang J, Ravi Shankar M, Chandrasekar S, Compton WD (2006) Metall Mater Trans A37:1633
16. Steeds JW (1966) Proc Royal Soc London A292:343
17. Hirsch J, Lucke K, Hatherly M (1988) Acta Metall 36:2905
18. Dalla Torre F, Lapovok R, Sandlin J, Thomson PF, Davies CHJ, Pereloma EV (2004) Acta Mater 52:4819
19. Belyakov A, Sakai T, Miura H, Tsuzaki K (2001) Phil Mag 81:2629
20. Ferrasse S, Segal VM, Hartwig KT, Goforth RE (1997) J Mater Res 12:1253
21. Zhao YH, Liao XZ, Jin Z, Valiev RZ, Zhu YT (2004) Acta Mater 52:4589
22. Kim WJ, Chung CS, Ma DS, Hong SI, Kim HK (2003) Scripta Mater 49:333
23. Kelly A, MacMillan NH (1986) Strong solids. Clarendon, Oxford, UK, 222 pp and 373 pp
24. Lu J, Ravichandran G, Johnson WL (2003) Acta Mater 51:3429
25. Kim JJ, Choi Y, Suresh S, Argon AS (2002) Science 295:654
26. Chen H, He Y, Shiflet GJ, Poon SJ (1994) Nature 367:541
27. Hwang J, Kompella S, Chandrasekar S, Farris TN (2003) ASME J Tribol 125(2):377
28. Humphreys FJ, Hatherly M (1996) Recrystallization and related annealing phenomena. Pergamon, 364 pp and 391 pp
29. Ravi Shankar M, Chandrasekar S, King AH, Compton WD (2005) Mater Sci Eng A 410–411:365